Role of the Metal Ion in Formyl−Peptide Bond Hydrolysis by a Peptide Deformylase Active Site Model

Monica Leopoldini, Nino Russo,* and Marirosa Toscano

Dipartimento di Chimica and Centro di Calcolo ad Alte Prestazioni per Elaborazioni Parallele e Distribuite—Centro d'Eccellenza MIUR, Universita' della Calabria, I-87030 Arcavacata di Rende, Italy

Received: August 31, 2005; In Final Form: October 31, 2005

The catalytic mechanism of peptide deformylase enzymes containing zinc, iron, cobalt, and nickel dications was explored in the gas phase and in the protein environment. The study was performed at the density functional level using three model systems to simulate the active site. The work had the aim to evaluate the effect of metal substitution on the hydrolytic properties and the possible different performances of the various catalysts. Results indicated that all of the metallic forms are active to hydrolyze the formyl−peptide bond and that the reaction pathways do not show significant peculiarities on going from a particular metal ion to another. No significant modification of the reaction paths occurs in solvent.

Introduction

Protein synthesis in prokaryotes begins with a formylmethionine at the N-terminus.[1,2] During the elongation of the polypeptide chain, the formyl group is hydrolytically removed by the enzyme peptide deformylase (PDF, EC 3.5.1.31). This posttranslational deformylation of peptides is a unique feature of bacterial cells, and it is essential for their survival. Since this formylation/deformylation cycle does not occur in eukaryotic protein synthesis, peptide deformylase may be a potential target for designing new antibiotics.[3,4]

Characterization by overexpression of the deformylase gene in *Escherichia coli*[5,6] revealed the presence of a typical zinc-binding motif, HEXXH (H = histidine, E = glutamate, X = any amino acid).[7−9] The purified enzyme contained approximately one metal ion per polypeptide, whose nature, however, was not well established. On the basis of gel filtration, anion exchange, and hydrophobic interaction chromatographic studies,[5,6] it was suggested that peptide deformylase belonged to the zinc hydrolase superfamily. However, these preparations were of a very low hydrolytic activity using formyl-Met-Ala-Ser as a substrate.[6] Other researchers found a higher activity in purified enzyme preparations that contained zinc and some varying amounts of other metals (Fe, Co, or Cu),[10] postulating that another metal ion besides zinc is responsible for this higher activity.

Recently, biochemical studies[11,12] suggested that peptide deformylase represents a new class of metallopeptidases, in which the catalytic ion is a ferrous rather than a zinc ion. The Fe(II)-containing form was very unstable because of its sensibility toward environmental oxygen.[13] To generate stable PDF variants, several researchers have replaced the Fe^{2+} ion with Ni^{2+} and Co^{2+} as well as Zn^{2+}. Whereas the zinc form showed reduced activity, the Ni^{2+} and Co^{2+} forms retained the same catalytic activity of the native enzyme, being also very stable.[10−12,14,15]

All the four metal forms share the same overall structure. Site-directed mutagenesis,[14] X-ray crystallography,[16] and nuclear magnetic resonance spectroscopy[17] studies revealed that the metal ion has a tetrahedral coordination sphere (Chart 1). The ligands are the γ-S-atom of a cysteine residue (Cys90), the ϵ2-N-atoms of two histidines (His132 and His136), and the oxygen atom of a water molecule. The glutamate residue, Glu133 of the HEXXH motif, does not bind the metal, but it is required for catalysis. In fact, mutations of this residue to Ala, Asp, or Gln result in a catalytically inactive protein.[7,14]

CHART 1: Employed Models

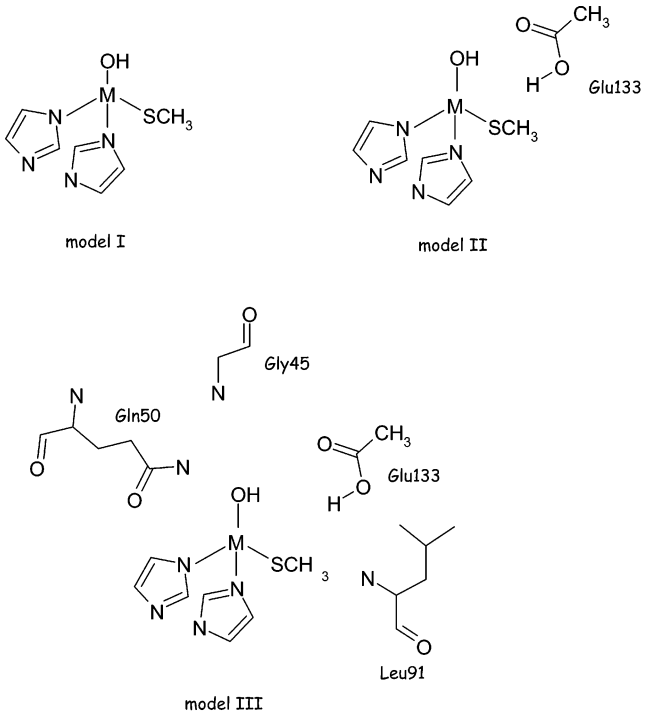

The catalytic cycle proposed for peptide deformylase[18] (Scheme 1) is similar to that suggested for other zinc metallopeptidases such as thermolysin[17] and carboxypeptidase A.[19] The formylated peptide binds the metal through the carbonyl oxygen of the formyl group, yielding an enzyme−substrate complex. The carbonyl oxygen is polarized by hydrogen bonds with the amide group of Leu 91 and the side chain of Gln50,

* Author to whom correspondence should be addressed. E-mail: nrusso@unical.it.

10.1021/jp054923y CCC: $33.50
Published on Web 12/22/2005

SCHEME 1: Proposed Catalytic Cycle

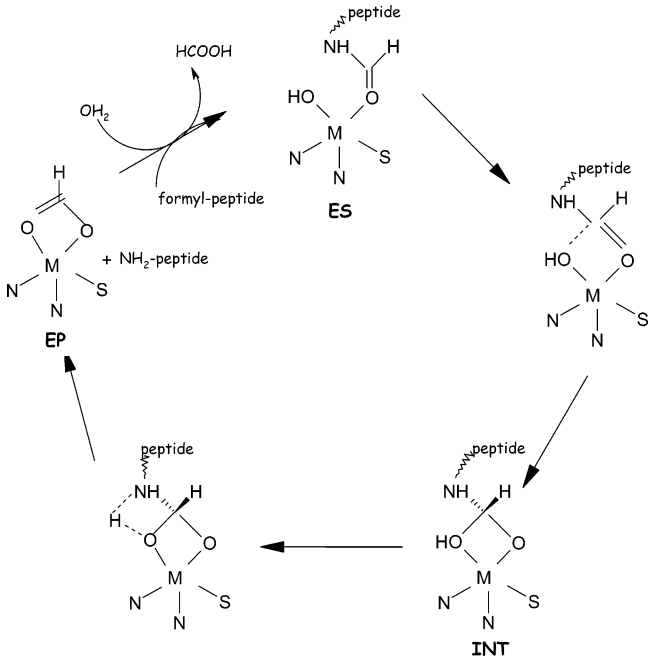

while the −NHR group in the substrate interacts with the carbonyl oxygen of Gly45. This supports the nucleophilic attack of the metal-bound water/hydroxide on the carbon of the formyl group, which leads to a tetrahedral intermediate. The proton of the hydroxide is then transferred to the amide at the N-terminus, with the probable aid of Glu133.[18] The protonation of the amide group determines the C−N bond cleavage. The formate appears to be bound to the metal, and the free N-terminus is linked to Glu133 by a hydrogen bond. The reaction proceeds toward the release of the formate upon the binding of an incoming water molecule with the metal.

In this work, we present for the first time a detailed density functional study of the hydrolysis of a formamide substrate by different metal forms (Zn(II), Fe(II), Ni(II), and Co(II)) of peptide deformylase active site models, according to the mechanism suggested in the literature for this enzyme. The aim of this investigation is to elucidate the catalytic function of metal ions using realistic active site models that include first shell metal ligands. The role of Glu133 as a proton shuttle is analyzed in a model in which this residue is simulated by a molecule involving a carboxylic functionality. The influence of the Gly45, Gln50, and Leu91 residues in substrate polarization is also analyzed.

Computational Details

The models used to study the catalytic mechanism of peptide deformylase were built up starting from the crystal structures available in the Protein Data Bank. We focused on the nucleophilic attack and on the proton-transfer processes involving the tetrahedral intermediate.

The three active site model systems reported in Chart 1 were employed. Model I consists of a divalent metal ion (Zn, Fe, Ni, or Co) coordinated to two imidazole rings and to a $-SCH_3$ group that simulate the histidine (His132 and His136) and the cysteine (Cys90) residues, respectively. In model II, an acetic acid molecule is added in the active site immediate vicinity to emulate the Glu133 residue. In model III, Gly45, Gln50, and Leu91 were further added to provide the hydrogen-bonding network involved in substrate binding. As in previous studies,[19] the peptide substrate was modeled by a formamide molecule. The nucleophilic attack on formamide was provided by the metal-bound hydroxide rather than the metal-bound water molecule, owing to the fact that the first species is generally accepted to be the nucleophile.[19,20] This is not surprising if we take into account the increased acidity of H_2O when coordinated to a transition metal ion.

All of the computations reported here were carried out with the Gaussian 03 code,[21] employing the hybrid Becke exchange and Lee, Yang, and Parr correlation (B3LYP)[22,23] functionals. The performance of the density functional theory B3LYP method in predicting the properties of transition-metal-containing systems is satisfactory and supported by a large amount of literature concerning enzymatic catalysis.[19,20,24−32] The 6-31+G* basis set[33−36] was chosen for the C, S, N, O, and H atoms, while for the metals the LANL2DZ pseudopotential[37] was used.

No constraints were imposed during the optimization of model systems I and II. In the largest model (71 atoms), model III, the coordinates of one atom of each residue (Gly45, Gln50, Leu91, Cys90, His132, His136, and Glu133) were kept frozen to their crystallographic position to avoid an unrealistic expansion of the protein. The substrate was left without any constraint during the optimization.

Frequency calculations were performed at the same level of theory on the stationary points of all reaction paths with the aim to evaluate their character of minima and saddle points. Zero point energy corrections, obtained from the vibrational frequencies, were then included in all of the relative energy values. With the aim to confirm that a given transition state connects reactants and products, intrinsic reaction coordinate calculations were performed at the same level of theory for models I and II. In the case of larger model III, all attempts to use this scheme were unsuccessful owing to technical difficulties essentially due to the frozen positions of atoms.

Solvent effects were computed in the framework of a self-consistent reaction field polarized continuum model (SCRF-D-PCM)[38−40] using the UAHF[41] set of solvation radii to build the cavity for the solute in the gas-phase equilibrium geometries. The dielectric constant value $\epsilon = 4$ was chosen for describing the protein environment of the active site, according to previous suggestions for proteins.[31,32] The relative solvent effects between minima and transition states are normally calculated to be quite small, within 2 kcal/mol.[31,32] Usually, when large solvent effects are obtained, it is indicative of some deficiencies in the chemical model of the active site. It must be remembered that the consideration of protein environment as a simple continuum with average properties (like in D-PCM) obviously is a crude approximation in situations where appreciable interactions occur between subsystem and environment, with effects depending on their electronic structures.[40] However, the inclusion in the quantum model cluster of strongly localized and directional H-bonding interactions may reduce the anisotropic features of the protein environment,[41] making the solvation continuum models qualitatively good enough.

Results and Discussion

Ground-State Multiplicities. The complexes with the Zn^{2+} transition metal ion, which has a d^{10} electron configuration, are closed-shell systems characterized by the singlet ground state.

In their tetrahedral complexes, Fe^{2+} (d^6), Co^{2+} (d^7), and Ni^{2+} (d^8) may exist in more than one spin state. Ni^{2+} and Co^{2+} can be found in a low-spin and a high-spin state (singlet and triplet for Ni^{2+}, doublet and quartet for Co^{2+}), whereas Fe^{2+} may exists in three spin states, i.e., singlet, triplet, and quintet.

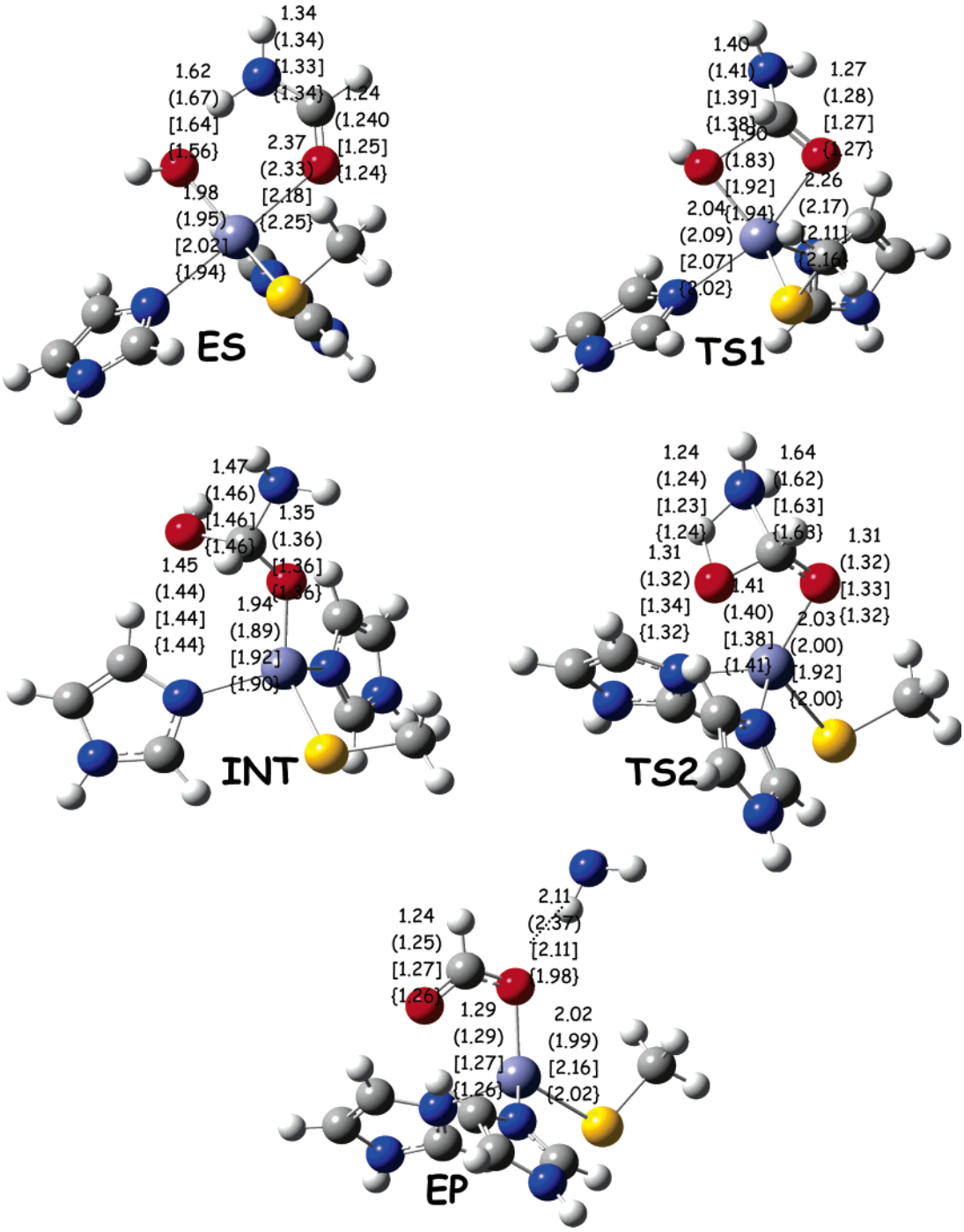

Figure 1. Optimized geometries of ES, TS1, INT, TS2, and EP points for Zn-, (Fe)-, [Ni]-, and {Co}-containing model I. Distances are in angstroms.

Because no experimental study exists on the determination of the magnetic susceptibility of the Fe^{2+}–, Ni^{2+}–, and Co^{2+}–peptide deformylase, we have considered distinct spin multiplicities for each of these enzymes and carried out a full optimization analysis, with the aim to determine the electronic ground state and to predict the best ligands arrangement around the transition metal as in the X-ray crystal structure.

For the Fe^{2+} complex, a ground state of the quintet was found, with the triplet and singlet states lying at 54.6 and 96.9 kcal/mol, respectively. The complex in the quintet state shows tetrahedral coordination.

The energetic gap between the singlet and the triplet states for the Ni^{2+} complex was found to be only 2.5 kcal/mol, being the triplet the ground state. As expected with Ni^{2+} in the singlet state, the complex shows a square-planar geometry, whereas tetrahedral coordination is favored when the metal ion assumes the triplet electronic state.

For Co^{2+}, the high-spin quartet state lies 6.0 kcal/mol below the doublet one. The high-spin complex is in a tetrahedral arrangement, whereas the low-spin one shows a planar disposition.

So, we have concluded that the high-spin states are likely to be involved in all the metal forms of peptide deformylase, except obviously for the zinc-containing one.

Role of the Metal Substitution. The following discussion refers to the simulation with model I.

The first step in the catalytic reaction (Scheme 1) is the barrierless formation of a complex (ES) between the active site and the substrate. Irrespective of the metal center, ES is characterized by a bond between the carbonyl oxygen of

formamide and the M^{2+} ion that becomes five-coordinated (Figure 1). Upon this interaction, the C═O bond in the substrate is polarized. The −OH lone pair interacts with the $-NH_2$ terminal group of the substrate, establishing a hydrogen bond of 1.62, 1.67, 1.56, and 1.64 Å, for zinc, iron, nickel, and cobalt, respectively. Important equilibrium distances are collected in Tabls S1 in the Supporting Information.

A similar binding mode of the peptide substrate occurs in several metallopeptidases.[19,20]

The transition state TS1 for the nucleophilic attack of hydroxyl on the carbonyl carbon atom of formamide is reached when the HO−C_{sub} distance (the subscript refers to atoms in the initial substrate) assumes the values of 1.90 (Zn^{2+}), 1.83 (Fe^{2+}), 1.92 (Ni^{2+}), and 1.94 Å (Co^{2+}) in the different metallic forms of the enzyme (Figure 1). Imaginary frequency values of 257 (Zn^{2+}), 306 (Fe^{2+}), 253 (Ni^{2+}), and 292 (Co^{2+}) cm^{-1} correspond to the stretching of the HO−C_{sub} forming bond. The OH group remains still coordinated to the metal although the M^{2+}−OH distances are quite longer with respect to those of initial complex. At the same time, the C−N and O_{sub}−C_{sub} bonds lengthen on average (considering all four metals) 0.06 and 0.03 Å, respectively, in going from ES to TS1.

The TS1 transition state leads to a stable intermediate, INT, in which the bond between the oxygen of the hydroxide and the carbon of the formamide is completely formed (the HO−C_{sub} average distance is ∼1.44 Å). The carbon of the substrate changes its hybridization from sp^2 to sp^3, as confirmed by the N_{sub}−C_{sub} and O_{sub}−C_{sub} average distances (∼1.46 and ∼1.36 Å, respectively). The M^{2+} goes back to being four-coordinated after the cleavage of the bond between the OH group and the metal.

The next step in the reaction is the proton transfer from the hydroxide to the amide nitrogen. The process occurs through a transition state (TS2) in which the proton is partially bound to both the oxygen and the nitrogen atoms (the O−H and OH−N_{sub} average distances are ∼1.32 and ∼1.24 Å, respectively). The imaginary vibrational mode whose frequency is 1628 (Zn^{2+}), 1635 (Fe^{2+}), 1643 (Ni^{2+}), and 1636 (Co^{2+}) cm^{-1}, respectively, sees the hydrogen atom moving between two atoms. The coordination number around the metal practically does not change even if the M^{2+}−O bond appears to be sensibly shorter than that in INT.

The proton is fully transferred to the nitrogen (∼1.04 Å) in the final complex EP. The C−N bond is completely broken, changing on average from ∼1.63 Å in TS2 to ∼3.52 Å in the product. The ammonia leaving group is still held at about 2.00 Å by a hydrogen bond with the formate oxygen, and the metal is four-coordinated to the imidazole rings, to the SCH_3 group, and to one of the oxygen atoms of the formate product. The formate is coordinated to the metallic center through a bond whose average value is 2.05 Å.

The potential energy profiles obtained for zinc, iron, nickel, and cobalt are depicted in Figure 2. The reaction appears to be exothermic since the enzyme−product complex EP is lower in energy than the initial complex ES in all the four cases.

The energetics of the hydrolysis obtained at the B3LYP level are quite similar in going from zinc to cobalt, and the particular metal does not seem to affect drastically the catalysis as suggested on the basis of experimental determinations.[10,12,13] The nucleophilic attack requires 22.4, 21.8, 19.8, and 22.6 kcal/mol in the case of zinc, iron, nickel, and cobalt, respectively. The rate-limiting step can be recognized in the proton-transfer process that converts INT into EP. It requires an amount of energy of 24.4 (Zn^{2+}), 25.7 (Fe^{2+}), 28.2 (Ni^{2+}), and 26.3 kcal/mol (Co^{2+}), when computed with respect to the intermediate INT.

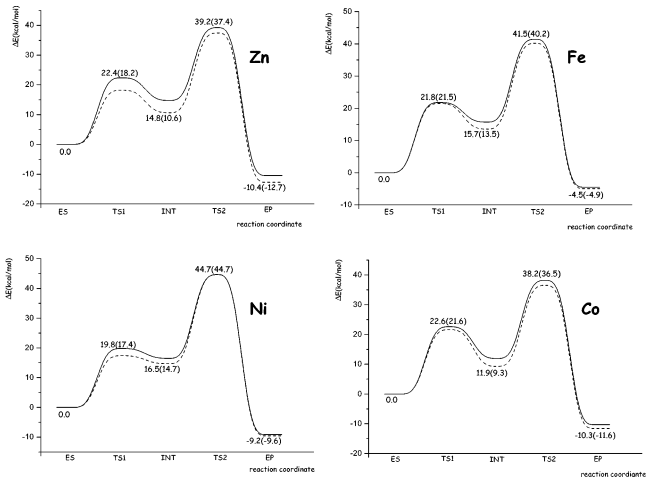

Figure 2. Gas-phase (solid line) and solvated (dash line) potential energy profiles for Zn-, Fe-, Ni-, and Co-containing model I. Values are in kcal/mol.

Single-point estimations of the solvation energy using the gas-phase B3LYP equilibrium structure for the different metallic forms of the enzymes were performed. A continuum dielectric constant of 4 was chosen since, as indicated in some previous works concerning the enzymatic catalysis,[31,32] this value can describe reliably the combined effect of a protein embedded in a water solution on the solute.

The paths obtained taking into account the protein environment are reported together with gas-phase profiles for each metal cation (see dashed lines of Figure 2). As it is evident, no substantial modification occurs in the solvent. The aspect common to all cases is the stabilization of both intermediates and transition states. This means that the heights of the rate-limiting step barriers remain almost the same as those in the gas phase.

Role of the Glu133 Residue. Glu133 is the second residue in the HEXXH motif, which is highly conserved among all peptidedeformylases. Its role was suggested on the basis of mutation studies[43] in which it was replaced by alanine, aspartate, cysteine, and glutamine. Only the E133D mutant containing the aspartate functionality, was catalytically active, whereas the others were totally inactive toward hydrolysis.[43]

Glu133 is accepted to act as a general base by abstracting one proton from the metal-bound water molecule and to facilitate the product release by protonating in turn the −NHR group in the formed tetrahedral intermediate.[43] Because the pK_a values for the metal-bound water (∼6.5) and the carboxyl group of Glu133 (∼5) are similar, the shared proton may be readily transferred from the water molecule to the carboxylate generating the metal-bound hydroxide, which can perform the attack on the peptide carbonyl carbon. This is supported by the experimental findings that aspartate, contrary to the mutants in which no carboxylate groups are present, is still active.[43] No other nearby residues may function in such a way.

To corroborate the role played by Glu133, we have studied the catalysis toward formamide hydrolysis with a second model (referred to as model II in Chart 1) enlarged by an acetic acid molecule modeling the Glu133 residue.

It must be remembered that the glutamate residue probably exists in a deprotonated state at neutral pH, but the carboxylate group of Glu133 should be protonated during the formation of

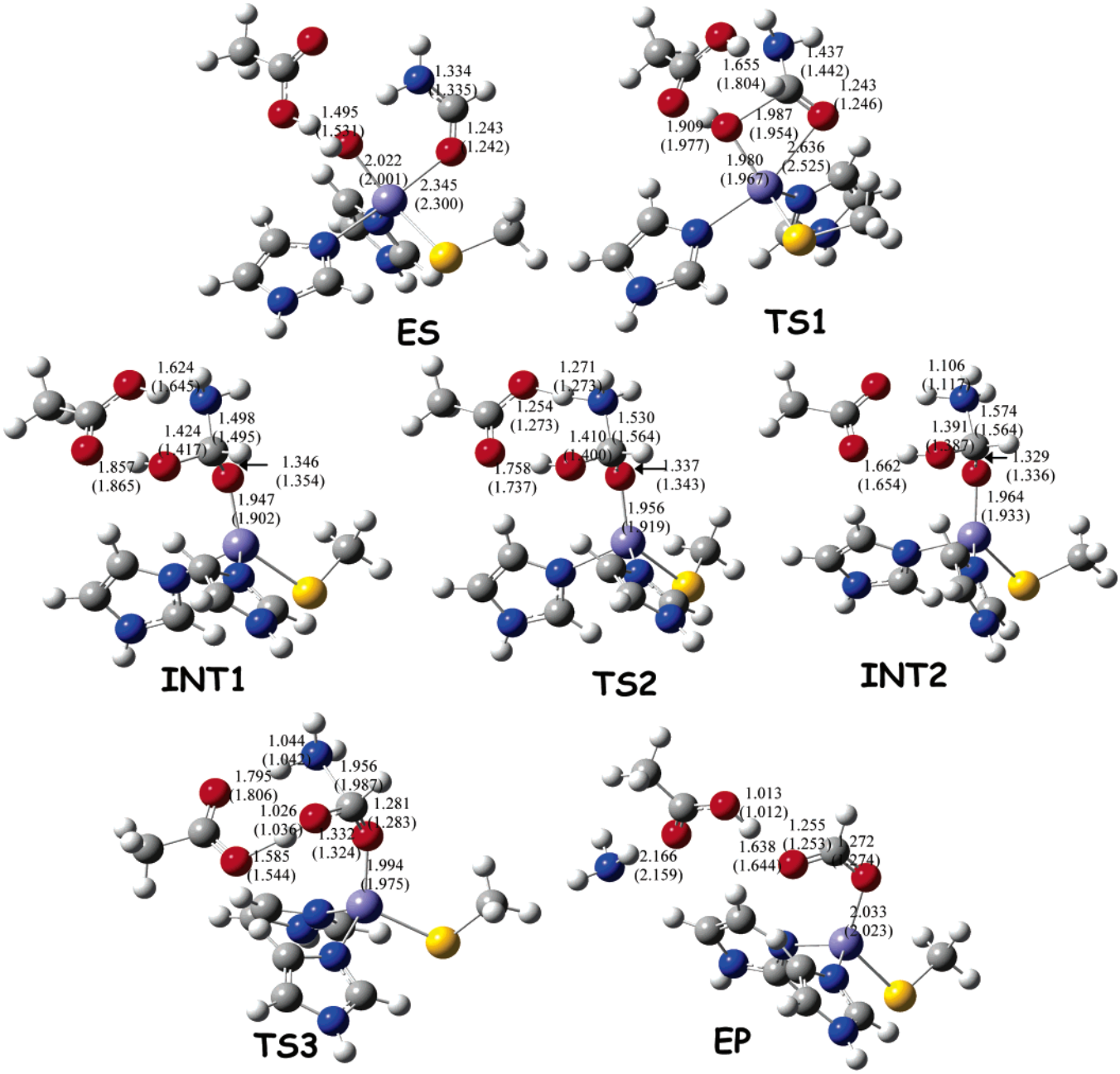

Figure 3. Optimized geometries of ES, TS1, INT1, TS2, INT2, TS3, and EP points for Zn- and (Fe)-containing model II. Distances are in angstroms.

the zinc-bound hydroxide. This has been elucidated in a theoretical study performed on carboxypeptidase A[19] in which a barrierless process has been observed for the shift of a proton from the water coordinated to the Zn atom toward the formate anion representing Glu270.

Computations with model II were performed for the Zn- and the Fe-containing enzymes because these two metal ions are the only candidates for an in vivo action of peptidedeformylase and thus have received major attention in the literature.[10,12,13,43]

The initial enzyme−substrate complex ES for model II is reported in Figure 3 (for distances, see Table S2 in Supporting Information). The substrate binds the metal by its carbonyl oxygen, as occurs in model I, and the metal-bound OH forms a hydrogen bond with the hydroxyl of acetic acid. The O_{sub}−M^{2+} distances are 2.34 and 2.30 Å, and the HO−HO_{Glu} hydrogen bond lengths (the subscript refers to atoms in glutamate) are 1.49 and 1.53 Å in the cases of zinc and iron, respectively. Both metal centers appear to be pentacoordinated.

The transition state (TS1) for the first ES → INT1 interconversion step occurs for an HO−C_{sub} distance value of 1.99 Å for zinc and 1.95 Å for iron. An imaginary vibrational mode (frequency at 303 (Zn^{2+}) and 229 (Fe^{2+}) cm^{-1}) clearly shows the formation of this new bond. The metal center results still linked to O_{sub} (Zn^{2+}−O_{sub} and Fe^{2+}−O_{sub} are 2.64 and 2.52 Å, respectively). By reason of the lengthening of the M^{2+}−O_{sub} distances, that leaves the metallic center in need of electrons, and the M^{2+}−OH bond shortens in both cases (Zn^{2+}−OH and Fe^{2+}−OH become of 1.98 and 1.97 Å, i.e., about 0.03 Å shorter than in ES). The Glu133 residue changes significantly its orientation with respect to that in the ES complex, as to establish a further hydrogen bond (1.65 Å for zinc and 1.80 Å for iron) in which the substrate nitrogen atom acts as an acceptor (Figure 3).

The transition state TS1 leads to a stable tetrahedral intermediate INT1 characterized by an HO−C_{sub} distance of 1.42 Å for both zinc and iron. Two hydrogen bonds stabilize INT1.

One of them involves the OH group of glutamate and the NH_2 lone pair (1.62 Å for zinc, 1.64 Å for iron); the other one occurs between the OH group of the substrate and the Glu133 carbonyl oxygen (1.86 Å for zinc and 1.86 Å for iron).

The next step is the protonation of the nitrogen atom that now, differently to what occurred in the description with model I, is mediated by the Glu133 hydroxyl. The protonation occurs through the transition state TS2, whose imaginary frequency at 773 and 691 cm^{-1} for zinc and iron, respectively, refers to the stretching vibrational mode of the $H_{Glu}-N_{sub}$ bond that is in formation. TS2 is a four-coordinated species whose geometrical features are very similar to those of the INT1 intermediate.

The proton shift leads to another intermediate INT2 in which the C−N bond is still present and the $H_{Glu}-N_{sub}$ bond is completely formed (1.11 Å for zinc and 1.12 Å for iron).

Finally, in TS3, characterized by an imaginary vibrational frequency of 215 (Zn^{2+}) and 223 (Fe^{2+}) cm^{-1}, the second proton is transferred from the OH group of the substrate to the carbonyl oxygen atom of glutamate. This H^+ transfer and the following shorthening of the $HO-C_{sub}$ bond (it changes from 1.39 Å in INT2 to 1.33 Å in TS3 in the case of zinc, and from 1.39 to 1.32 Å for iron) is the driving force that determines the C−N bond cleavage. The TS3 structure is characterized by the $N_{sub}-C_{sub}$ distance of 1.96 Å for zinc and 1.99 Å for iron and by a $OH-O_{Glu}$ distance of 1.58 Å for Zn and 1.54 Å for Fe.

In the final complex EP, ammonia appears to be bound to Glu133 through a hydrogen bond (2.17 and 2.16 Å for zinc and iron). The glutammic acid residue is again produced, and the formate group is strongly coordinated to the metallic center.

As can be noted, when model II is employed to study the hydrolysis reaction, an energetic scheme that is completely different from that of model I is obtained (Figure 4). The formation of the tetrahedral intermediate controls the reaction rate, with barriers of 33.2 kcal/mol in the case of zinc and 28.3 kcal/mol in the case of iron. The second step of the reaction requires now two protons to be transferred, demanding lower amounts of energy. First, one proton is transferred from the acetic acid molecule to the NH_2 group, crossing a maximum TS2 (that lies at only 1.3 and 1.9 kcal/mol above INT1, for zinc and iron, respectively) and yielding to a stable intermediate, INT2. The flatness of the reaction profile suggests that the INT1−TS2−INT2 conversion is very easy. Then, the other proton moves from the hydroxide to the other acetic acid oxygen atom through TS3, spending also in this case only 1.7 and 2.9 kcal/mol, for Zn- and Fe-containing systems, respectively.

The barrier heights for the H^+ transfers are very small when amino acids in the active site mediate them. Glu133 acts lowering the activation energy required for transferring the proton on the substrate nitrogen, with the intermediate collapsing easily to the final complex. Moreover, the glutamate is able to split the proton shift into two distinct processes requiring a smaller amount of energy than that required for a direct shift from the nucleophile to the nitrogen.

The role found here for Glu133 was already suggested for Glu270 in carboxypeptidase A,[19,44] for Asp120 in β-lactamases,[20] and for Thr199 and Glu106 in carbonic anhydrase.[45]

Also for model II no significant differences in achieving catalysis are observed in going from zinc to iron metal ions. Both are able to hydrolyze the formamide substrate through a mechanism composed of the same elementary steps and demanding a similar amount of energy.

Role of the Backbone Gly45, Gln50, and Leu91 Residues. The rate-limiting TS1 barriers of 33.2 and 28.3 kcal/mol, found for zinc and iron in model II, respectively, still seem to be too large to be acceptable for enzyme catalysis. This means that even if the required energy for the C−N cleavage is decreased by employing model II, some improvements must be done to our model to be valid enough to reproduce a reasonable energy associated to the nucleophilic addition step.

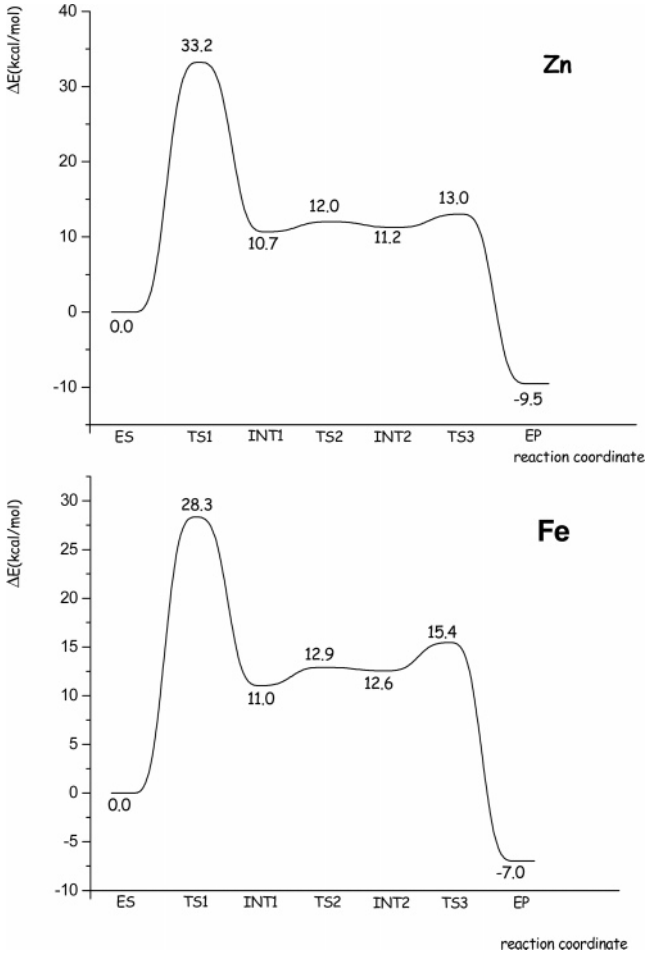

Figure 4. Potential energy profiles for Zn- and Fe-containing model II. Values are in kcal/mol.

By adding second-shell amino acids to the active site, one should reproduce the hydrogen-bonding network able to stabilize intermediates and transition states. This should lead to a decrease of the activation energy. The influence of electrophilic agents in proximity to the peptide hydrolysis was elucidated for thermolysin,[46] a Zn^{2+} peptidase catalyzing the hydrolysis of a peptide bond specifically on the imino side of large hydrophobic residues.[46] The authors of this work indicated a lowering of the hydrolysis barrier by about 10 kcal/mol when polar residues establishing hydrogen-like interactions with the substrate were included in the employed model.

So, a further model (model III in Chart 1) enlarged by the Gly45, Gln50, and Leu91 residues was used, for zinc and iron metals. Through the use of the geometries obtained for model II as starting points, related minima along the reaction pathway were optimized.

The enzyme−substrate complex (ES) (see Figure 5 and Table S3 in Supporting Information) is characterized by a pentacoordinated metal cation, simultaneously bound to the oxygen atoms coming from the nucleophile ($M^{2+}-OH$ distance is 2.07 Å for zinc, and 2.03 Å for iron) and the substrate ($M^{2+}-O_{sub}$ distance is 2.36 and 2.30 Å for zinc and iron, respectively). The comparison with the ES species obtained with model II shows that three additional stabilizing hydrogen bonds are

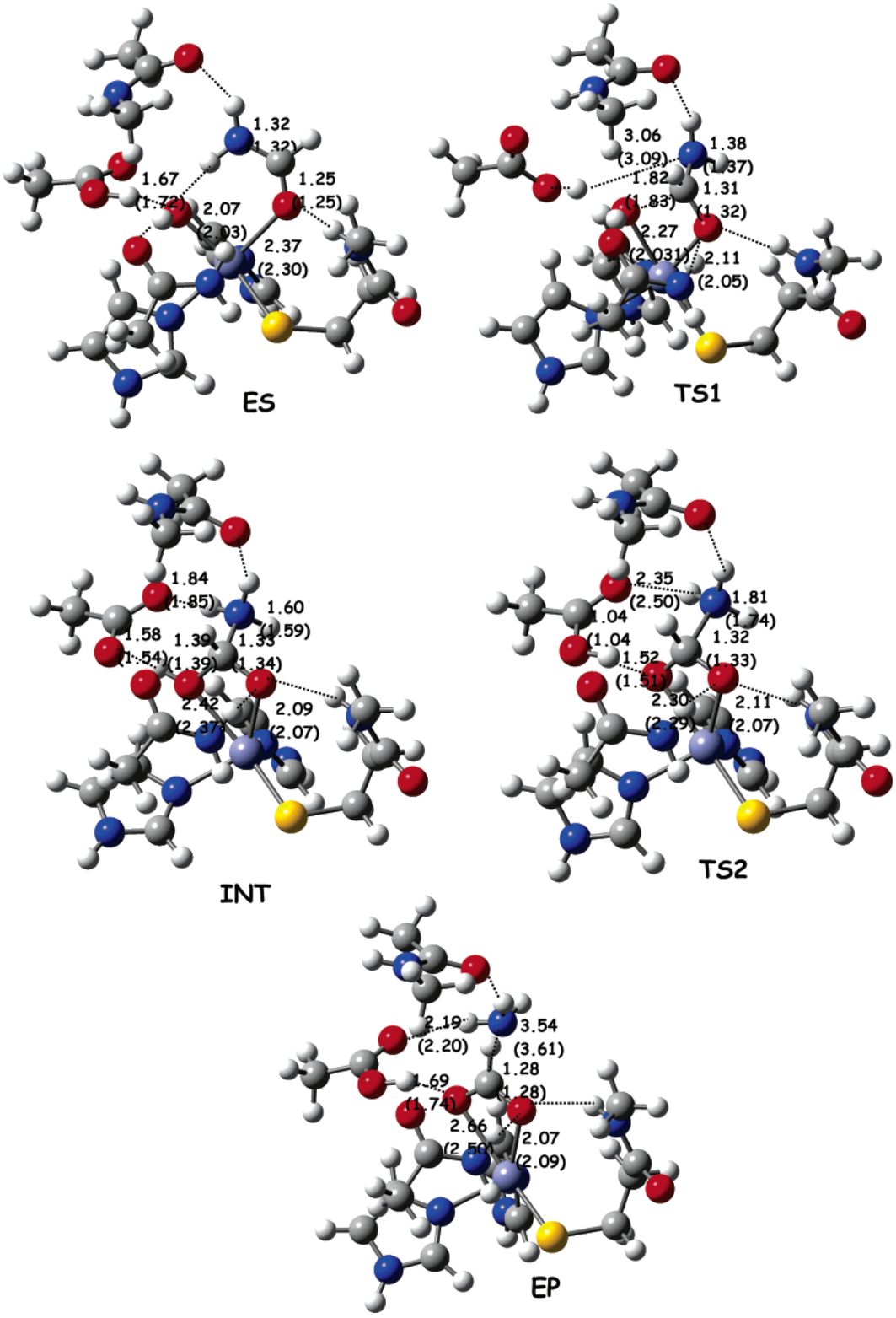

Figure 5. Optimized geometries of ES, TS1, INT, TS2, and EP points for Zn- and (Fe)-containing model III. Distances in angstroms.

present. These involve the NH_2 terminal and the carbonyl oxygen of Gly45 (2.01 Å for zinc and 2.02 Å for iron), the substrate oxygen and the NH of Leu91 (2.17 Å for zinc and 2.37 Å for iron), and the metal-bound hydroxide and the carbonyl oxygen of Gln50 (2.32 Å for zinc and 2.20 Å for iron). No significant differences are encountered in going from zinc to iron ES complexes.

At first glance, the transition state TS1 corresponds to the nucleophilic attack from the metal-bound hydroxide on the carbonyl carbon of formamide. It occurs for a $HO-C_{sub}$ distance of 1.82 Å for Zn^{2+} and 1.83 Å for Fe^{2+}. Consequently, the C−N and the C−O distances in the substrate lengthen up to 1.38 and 1.31 Å (Zn^{2+}) and up to 1.36 and 1.32 Å (Fe^{2+}). Vibrational analysis gave a low imaginary frequency at 297 cm^{-1} for zinc and at 291 cm^{-1} for iron, whose corresponding vibration mode indicates the simultaneous occurrence of the stretching of the heavy atoms in the $HO-C_{sub}$ bond and the approach of the hydroxyl of the Glu133 residue to the nitrogen atom of the NH_2

group of the substrate. The hydrogen bonds are retained passing from ES to TS1 species, while the Gln50 residue arranges itself to establish a quite strong hydrogen bond involving its NH_2 group and the substrate oxygen (the length is 2.00 Å for zinc and 2.02 Å for iron). All of these interactions polarize the formamide substrate and are important for the stabilization of the corresponding transition state TS1.

After this transition state, a tetrahedral intermediate along the reaction pathway was obtained. Surprisingly, no local minimum corresponding to that obtained with model II (i.e., INT2) and involving the formation of a NH_2-C σ-bond, was obtained.

The next point after TS1 along the model III reaction path is an intermediate that shows a protonated nitrogen atom and a stable hydroxyl−carbon bond in the substrate. This minimum resembles strongly INT2, encountered on the flat portion of the potential energy surface of model II, describing the proton-transfer process from the glutamate hydroxyl to the formamide nitrogen (i.e., by the INT1−TS2−INT2 conversion). So, in model III, TS1 seems to be responsible for both the nucleophilic attack and the proton-transfer steps, being mainly driven by the motion of heavy atoms. However, all attempts to localize a transition state related to TS2 of model II repeatedly failed when the most advanced model III was employed.

Similar conclusions were drawn for the rate-limiting nucleophilic attack in thermolysin,[46] for which a concerted transition state for both processes was proposed.

In this intermediate (INT in Figure 5), the carbon−nitrogen bond in the substrate is quite long (1.60 and 1.59 Å, for zinc and iron, respectively) as compared to a covalent C−N σ-bond. The substrate is doubly coordinated to the metallic center (M^{2+}−OH and $M^{2+}-O_{sub}$ distances are 2.42 and 2.09 Å, and 2.37 and 2.07 Å for zinc and iron, respectively). Because of the established hydrogen bonds with the substrate ($OH-O_{Glu}$ and $O_{Glu}-H_{NH_2}$ distances are 1.57 and 1.84 Å in the case of Zn^{2+}, and 1.54 and 1.85 Å in the case of Fe^{2+}), the unprotonated Glu133 residue is fixed at a good position to accept the hydroxyl proton.

The conversion of INT into the product complex EP occurs via the transition state TS2, whose optimized structure is shown in Figure 5. The unprotonated Glu133 group easily takes the proton from the hydroxide ($O_{Glu}-HO$ distance is 1.04 Å, for both zinc and iron cations). Consequently, the $C_{sub}-N_{sub}$ bond lengthens up to 1.81 Å (Zn^{2+}) and 1.74 Å (Fe^{2+}).

The final complex EP shows a formate group coordinated to the metal cation, with a protonated glutamate residue and ammonia molecule interacting with the Gly45 and Glu133 residues via two hydrogen bonds. Formate is involved in a hydrogen-bonding network with Leu91 NH, Gln50 NH_2, and Glu133 carbonyl groups, respectively, for both zinc and iron cations.

Recently, the X-ray structures of Fe−, Co−, and Zn−PDF in complex with formate were determined at 1.85, 1.30, and 1.76 Å resolutions, respectively.[47] In all of the structures, the metal-bound formate establishes several hydrogen bonds, with the backbone NH of Leu91 and the side chains of Gln50 and Glu133. However, a difference in the formate binding mode was encountered for Zn and Fe complexes. In fact, with Fe−PDF, formate binds the metal in a bidentate fashion, with M^{2+}−O(formate) distances of 2.44 and 2.30 ± 0.17 Å. In Zn−PDF, only one oxygen of formate binds zinc (2.09 ± 0.17 Å), while the second one is located at a distance of 2.88 Å from the metallic center.

TABLE 1: Atomic Net Charges (in |e|) Obtained by NBO Analysis for the Species Encountered in Zn- and Fe−PDF Model III Energy Profiles

	zinc	iron
	ES	
M^{2+}	1.649	1.421
O_{OH}	−1.307	−1.251
O_{sub}	−0.771	−0.747
C_{sub}	0.509	0.509
N_{sub}	−0.845	−0.847
	TS1	
M^{2+}	1.640	1.390
O_{OH}	−1.064	−1.038
O_{sub}	−0.941	−0.901
C_{sub}	0.512	0.511
N_{sub}	−0.899	−0.886
	INT	
M^{2+}	1.605	1.360
O_{OH}	−0.890	−0.888
O_{sub}	−0.975	−0.927
C_{sub}	0.544	0.546
N_{sub}	−0.894	−0.890
	TS2	
M^{2+}	1.604	1.360
O_{OH}	−0.951	−0.939
O_{sub}	−0.948	−0.921
C_{sub}	0.578	0.566
N_{sub}	−0.963	−0.927
	EP	
M^{2+}	1.599	1.345
O_{OH}	−0.878	−0.827
O_{sub}	−0.793	−0.792
C_{sub}	0.653	0.651
N_{sub}	−1.188	−1.186

In the EP complex in Figure 5, formate binds the two metals differently. In particular, Zn appears to be tetracoordinated, with one oxygen atom of formate at 2.07 Å while the other is mainly involved in a strong hydrogen bond with the Glu133 OH group ($Zn^{2+}-O_{formate}$ distance is 2.66 Å). The Fe^{2+} EP complex shows a pentacoordinated metal with formate oxygen atoms at distances of 2.09 and 2.50 Å from Fe^{2+}, respectively. Our results are in quite good agreement with the experimental indications,[47] even if one has to note that our model for the enzyme−formate−ammonia complex includes a protonated Glu133 residue while an unprotonated residue is experimentally detected.

Experimentalists[47] hypothesized that the different binding modes for zinc and iron peptide deformylase found in the products may occur along the whole reaction path and can be recognized as the key reason for the better catalysis of iron with respect to zinc enzyme. In fact, because the metal serves as a Lewis acid and an electron-withdrawing group polarizing both nucleophile and substrate, the stronger the hydroxide− and substrate−metal interactions, the more active the metal should be.

B3LYP results indicate that, except for a slight difference in EP, the binding mode of the substrate and the nucleophile in all species along the path is quite similar in going from Zn^{2+} to Fe^{2+} cation (see optimized structures in Figure 5), so that the induced substrate polarization is quite similar for both metals. Table 1 lists the natural charges for the zinc and iron encountered in model III species, obtained by natural bond orbital (NBO) analysis, which can give some indication about the measure of substrate activation.

The natural charge on Zn^{2+} appears to be higher than that of iron, especially for ES and TS1 (Table 1). Because of this, one would expect that Zn enzyme would be more active than the

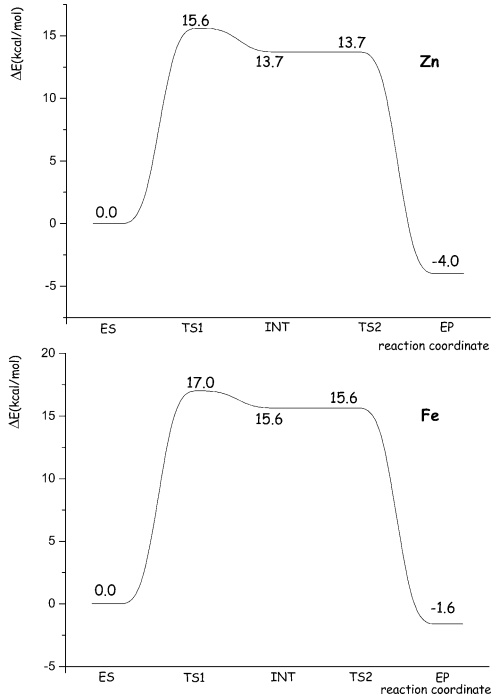

Figure 6. Potential energy profiles for Zn- and Fe-containing model III. Values are in kcal/mol.

Fe homologue. Instead, natural charges show that metal-induced polarization on the substrate is quite similar for both of the metallic forms.

Figure 6 reports the potential energy profiles for zinc and iron cations obtained by employing model III. The nucleophilic addition on the substrate carbon is the rate-limiting step, requiring an activation energy of 15.6 and 17.0 kcal/mol for Zn^{2+} and Fe^{2+}, respectively. The INT species are at 13.7 and 15.6 kcal/mol above the ES minimum. The transition state TS2 is responsible for both the heterolytical dissociation of the $C_{sub}-N_{sub}$ bond and for the H^+ transfer from the OH nucleophile to the oxygen atom of the Glu133 residue. A feature of the model III energetic profile is that the Zn and Fe TS2 lie more or less at the same energy of the INT species. This can be translated into a *single-step* mechanism for peptide deformylase, as it occurs for other metallopeptidases.[46]

Products are found at 4.0 and 1.6 kcal/mol below the ES energy, for zinc and iron, respectively.

Upon comparison between the potential energy surfaces obtained for models II and III, it is worthwhile to note that the presence of additional amino acids surrounding the active site in model III drastically decreases the energy of the rate-determining transition state TS1, passing from 33.2 to 15.6 kcal/mol and from 28.3 to 17.0 kcal/mol, for zinc and iron, respectively. Furthermore, the H^+ transfer process from the Glu133 OH to the NH_2 group in the substrate becomes concerted with the nucleophilic attack. Finally, the C−N bond cleavage, mediated by H^+ movement from the OH to the Glu133 carboxyl group in the intermediate, becomes a barrierless process, implying that once the TS1 is overtaken the tetrahedral complex directly collapses into products.

Our results are qualitatively and quantitatively in good agreement with data coming from other metallopeptidases, for example, for zinc-containing thermolysin,[46] for which the nucleophilic attack was found to have an activation energy of 15.2 kcal/mol, fitting the experimental value of 12.4−16.3 kcal/mol.

No peculiar differences are found between zinc and iron catalytic metals employing model III. In fact, the energy cost for peptide hydrolysis is almost the same in both cases.

Our findings appear to be in disagreement with the scarce catalytic activity of zinc in peptide deformylase as proposed by Rajagopalan.[12] The experimentally determined catalytic activities[6,10,12] that so much provided conflicting results seem to depend on the assay conditions and purification procedures. In fact, some researchers[7] reported a high activity immediately after cell lysis but a lower activity during purification steps. High levels of peptide concentration are reported to cause PDF inhibition,[6] claiming that the poor catalytic ability of the Zn−enzyme previously purified was mainly due to an inadequate activity assay involving substrate concentration and precipitation. Support to our results arises from the recent discovery of bacterial deformylases whose Zn forms are almost as active as their Fe homologues.[48]

Conclusions

We have investigated at the B3LYP level of theory how small but reliable active site models of peptide deformylase can catalyze the hydrolytic cleavage of the formyl−peptide bond. Our results indicate that the whole reaction is composed by two different steps, the nucleophilic attack on the substrate carbonyl carbon that leads to a stable tetrahedral intermediate and the protonation of the −NHR group of the peptide that determines the C−N bond to be broken.

Without any assistance by nearby residues, the proton-transfer process may be recognized as the rate-limiting step, demanding a higher amount of energy with respect to the first process. If it is assisted by Glu133, then the barrier decreases so it becomes lower than that required for the tetrahedral intermediate formation.

When the nearby residues Gly45, Gln50, and Leu91, whose role in substrate stabilization has been already claimed, are added, the rate-limiting hydroxide attack activation energy on the substrate carbonyl carbon decreases by ∼10 kcal/mol, reproducing a biologically reasonable reaction rate.

From our theoretical calculations, the substitution of the catalytic metal from zinc to iron, nickel, and cobalt seems to have a small effect on the reaction barriers; i.e., no significant differences occur when applying different metal-containing models.

The role of the M(II) seems to be that to generate the nucleophilic hydroxide from the metal-bound water and to polarize the carbonyl group when substrate approaches the metallic center. Zn, Fe, Ni, and Co seem to be able to perform these roles.

Perhaps the experimentally observed and supposed disparities in catalytic activities between Zn−PDF and Fe−PDF should be researched not in the metal ion itself but in other factors such as gene expression, enzyme purification, and technical conditions.

Acknowledgment. Financial support from the Università degli Studi della Calabria and Regione Calabria (POR Calabria 2000/2006, misura 3.16, progetto PROSICA) is gratefully acknowledged.

Supporting Information Available: Selected interatomic distances of the stationary points along the model I, II and III potential energy surfaces. This material is available free of charge via the Internet at http://pubs.acs.org.

References and Notes

(1) Kozak, M. *Microbiol. Rev.* **1983**, *47*, 1−45.
(2) Mazel, D.; Pochet, S.; Marliere, P. *EMBO J.* **1994**, *13*, 914−923.
(3) Meu, H. C. *Science* **1992**, *257*, 1064−1073.
(4) Gold, H. S.; Moellering, R. C., Jr. *N. Engl. J. Med.* **1996**, *335*, 1445−1453.
(5) Meinnel, T.; Blanquet, S. *J. Bacteriol.* **1993**, *175*, 7737−7740.
(6) Meinnel, T.; Blanquet, S. *J. Bacteriol.* **1995**, *177*, 1883−1887.
(7) Meinnel, T.; Lazennec, C.; Villoing, S.; Blamquet, S. *J. Mol. Biol.* **1997**, *267*, 749−761.
(8) Vallee, B. L.; Auld, D. S. *Biochemistry* **1990**, *29*, 5647−5659.
(9) Lipscomb, W. N.; Strater, N. *Chem. Rev.* **1996**, *96*, 2375−2433.
(10) Rajagopalan, P. T. R.; Datta, A.; Pei, D. *Biochemistry* **1997**, *36*, 13910−13918.
(11) Groche, D.; Becker, A.; Schlichting, I.; Kabasch, W.; Schultz, S.; Wagner, A. F. V. *Biochem. Biophys. Res. Commun.* **1998**, *246*, 342−346.
(12) Rajagopalan, P. T. R.; Yu, X. C.; Pei, D. *J. Am. Chem. Soc.* **1997**, *119*, 12418−12419.
(13) Rajagopalan, P. T. R.; Pei, D. *J. Biol. Chem.* **1998**, *273*, 22305−22310.
(14) Meinnel, T.; Lazennec, C.; Blamquet, S. *J. Mol. Biol.* **1995**, *254*, 175−183.
(15) Ragusa, S.; Blanquet, S.; Meinnel, T. *J. Mol. Biol.* **1998**, *280*, 515−523.
(16) Chan, M. K.; Gong, W.; Rajagopalan, P. T. R.; Hao, B.; Tsai, C. M.; Pei, D. *Biochemistry* **1997**, *36*, 13904−13909.
(17) Meinnel, T.; Blanquet, S.; Dardel, F. *J. Mol. Biol.* **1996**, *262*, 375−386.
(18) Groche, D.; Becker, A.; Schlichting, I.; Kabasch, W.; Schultz, S.; Wagner, A. F. V. *Nat. Struct. Biol.* **1998**, *5*, 1053−1058.
(19) Abashkin, Y. G.; Burt, S. K.; Collins, J. R.; Cachau, R. E.; Russo, N.; Erickson, J. W. In *Metal−Ligand Interactions: Structure and Reactivity*; Russo, N., Salahub, D. R., Eds.; Nato Science Series 474; Kluwer: Dordrecht, The Netherlands, 1996; pp 1−22.
(20) Olsen, L.; Anthony, J.; Ryde, U.; Adolph, H. W.; Hemmingsen, L. *J. Phys. Chem. B* **2003**, *107*, 2366−2375.
(21) Frisch, M. J.; Trucks, G. W.; Schlegel, H. B.; Scuseria, G. E.; Robb, M. A.; Cheeseman, J. R.; Montgomery, J. A., Jr.; Vreven, T.; Kudin, K. N.; Burant, J. C.; Millam, J. M.; Iyengar, S. S.; Tomasi, J.; Barone, V.; Mennucci, B.; Cossi, M.; Scalmani, G.; Rega, N.; Petersson, G. A.; Nakatsuji, H.; Hada, M.; Ehara, M.; Toyota, K.; Fukuda, R.; Hasegawa, J.; Ishida, M.; Nakajima, T.; Honda, Y.; Kitao, O.; Nakai, H.; Klene, M.; Li, X.; Knox, J. E.; Hratchian, H. P.; Cross, J. B.; Bakken, V.; Adamo, C.; Jaramillo, J.; Gomperts, R.; Stratmann, R. E.; Yazyev, O.; Austin, A. J.; Cammi, R.; Pomelli, C.; Ochterski, J. W.; Ayala, P. Y.; Morokuma, K.; Voth, G. A.; Salvador, P.; Dannenberg, J. J.; Zakrzewski, V. G.; Dapprich, S.; Daniels, A. D.; Strain, M. C.; Farkas, O.; Malick, D. K.; Rabuck, A. D.; Raghavachari, K.; Foresman, J. B.; Ortiz, J. V.; Cui, Q.; Baboul, A. G.; Clifford, S.; Cioslowski, J.; Stefanov, B. B.; Liu, G.; Liashenko, A.; Piskorz, P.; Komaromi, I.; Martin, R. L.; Fox, D. J.; Keith, T.; Al-Laham, M. A.; Peng, C. Y.; Nanayakkara, A.; Challacombe, M.; Gill, P. M. W.; Johnson, B.; Chen, W.; Wong, M. W.; Gonzalez, C.; Pople, J. A. *Gaussian 03*; Gaussian, Inc.: Wallingford, CT, 2004.
(22) Becke, A. D. J. *Chem. Phys.* **1993**, *98*, 5648−5652.
(23) Lee, C.; Yang, W.; Parr, R. G. *Phys. Rev. B* **1988**, *37*, 785−789.
(24) Hall, M. B.; Webster, C. E. *J. Am. Chem. Soc.* **2001**, *123*, 5820−5821.
(25) Friesner, R. A.; Beachy, M. D. *Curr. Opin. Struct. Biol.* **1998**, *8*, 257−262.
(26) Siegbahn, P. E. M.; Blomberg, M. R. A. *Annu. Rev. Phys. Chem.* **1999**, *50*, 221−249.
(27) Bernardi, F.; Bottoni, A.; Casadio, R.; Fariselli, P.; Rigo, A. *Int. J. Quantum Chem.* **1996**, *58*, 109−119.
(28) Bernardi, F.; Bottoni, A.; Casadio, R.; Fariselli, P.; Rigo, A. *Inorg. Chem.* **1996**, *35*, 5207−5212.
(29) Flock, M.; Pieloot, K. *J. Phys. Chem. A* **1999**, *103*, 95−102.
(30) Lind, T.; Siegbahn, P. E. M.; Crabtree, R. H. *J. Phys. Chem.* **1999**, *103*, 1193−1202.
(31) Siegbahn, P. E. M.; Blomberg, M. R. A. *Chem. Rev.* **2000**, *100*, 421−437.
(32) Noodleman, L.; Lovell, T.; Han, W. G.; Li, J.; Himo, F. *Chem. Rev.* **2004**, *104*, 459−508.
(33) Ditchfield, R.; Hehre, W. J.; Pople, J. A. *J. Chem. Phys.* **1971**, *54*, 724−728.
(34) Hehre, W. J.; Ditchfield, R.; Pople, J. A. *J. Chem. Phys.* **1972**, *56*, 2257−2261.
(35) Hariharan, P. C.; Pople, J. A. *Mol. Phys.* **1974**, *27*, 209−214.
(36) Gordon, M. S. *Chem. Phys. Lett.* **1980**, *76*, 163−168.
(37) Hay, P. J.; Wadt, W. R. *J. Chem. Phys.* **1985**, *82*, 270−283. Hay, P. J.; Wadt, W. R. *J. Chem. Phys.* **1985**, *82*, 284−298. Hay, P. J.; Wadt, W. R. *J. Chem. Phys.* **1985**, *82*, 299−310.
(38) Miertus, S.; Scrocco, E.; Tomasi, J. *Chem. Phys.* **1981**, *55*, 117−129.
(39) Miertus, S.; Tomasi, J. *Chem. Phys.* **1982**, *65*, 239−245.
(40) Cossi, M.; Barone, V.; Commi, R.; Tomasi, J. *Chem. Phys. Lett.* **1996**, *255*, 327.
(41) Barone, V.; Cossi, M.; Menucci, B.; Tomasi, J. *J. Chem. Phys.* **1997**, *107*, 3210−3221.
(42) Bottoni, A.; Lanza, C. Z.; Mkscione, G. P.; Spinelli, D. *J. Am. Chem. Soc.* **2004**, *126*, 1542−1550.
(43) Rajagopalan, P. T. R.; Grimme, S.; Pei, D. *Biochemistry* **2000**, *39*, 779−790.
(44) Bertini, I.; Luchinat, C. In *Bioinorganic Chemistry*; Bertini, I., Gray, H. B., Lippard, S. J., Valentine, J. S., Eds.; University Science Books: Mill Valley, CA, 1994.
(45) Marino, T.; Russo, N.; Toscano, M. *J. Am. Chem. Soc.* **2005**, *127*, 4242−4253.
(46) Pelmenschikov, V.; Blomberg, M. R. A.; Siegbahn, P. E. M. *J. Biol. Inorg. Chem.* **2002**, *7*, 284−298.
(47) Jain, R.; Hao, B.; Liu, E.; Chan, M. K. *J. Am. Chem. Soc.* **2005**, *127*, 4558−4559.
(48) Serero, A.; Giglione, C.; Meinnel, T. *J. Mol. Biol.* **2001**, *314*, 695−708.